

# Effect of cooling rates on sinter-hardened steels

L.A. Dobrzański\*, M. Musztyfaga

Division of Materials Processing Technology, Management and Computer Techniques in Materials Science, Institute of Engineering Materials and Biomaterials, Silesian University of Technology, ul. Konarskiego 18a, 44-100 Gliwice, Poland

\* Corresponding author: E-mail address: leszek.dobrzanski@polsl.pl

Received 24.09.2009; published in revised form 01.12.2009

## Manufacturing and processing

### ABSTRACT

**Purpose:** Purpose of this paper was to evaluate the differences between rapid, medium and low cooling rates on three systems and also to study cooling mechanism of known materials.

**Design/methodology/approach:** Two different systems have been tested in order to investigate how the cooling rates influence on the microstructure and properties. The powders used in the present invention are pre-alloyed iron-base powders containing low amounts of chromium and molybdenum. The amount of graphite that was admixed to the iron-base powder was 0.6% and lubricant 0.75%. The amount of graphite which is mixed with the iron-base powder is 0.6% and lubricant is 0.75%. Green compact were sintered in a vacuum furnace at 1120°C for 30 minutes in vacuum atmosphere and rapidly cooled in nitrogen with three different rates: rapid cooling (7°C/s) and medium cooling (1.6°C/s), slow cooling (0.3°C/s). Next the samples were tempered in vacuum in the same furnace at 200°C for 60 minutes and then were cooled to room temperature in nitrogen, with the exception of slow cooling cycle.

**Findings:** The effect of cooling and applied sintering were studied in terms of mechanical properties, hardness and wear resistance. The results achieved after the investigation sinter-hardened steels with low carbon content proved that applied process of sintering and different cooling rates brought expected outcome.

**Practical implications:** According to the powders characteristic, the applied rapid and medium cooling rate seems to be a good compromise for mechanical properties and microstructure, nevertheless further tests should be carried out in order to examine different cooling rates.

**Originality/value:** The effect of cooling rates on mechanical properties of pre-alloyed Astaloy CrL and CrM powders was investigated.

**Keywords:** Powder metallurgy; Sintering; Sinter-hardening

#### Reference to this paper should be given in the following way:

L.A. Dobrzański, M. Musztyfaga, Effect of cooling rates on sinter-hardened steels, Journal of Achievements in Materials and Manufacturing Engineering 37/2 (2009) 630-638.

## 1. Introduction

Powder metallurgy is a technology and craft of producing metal powders and of the utilization of metal powders for the production of massive materials and complicated shape objects

[1,2]. The growth of the P/M industry during the past few decades is considerably growing thanks to the cost savings associated with net shape processing compared to other technologies, such as casting or forging [3]. There are two principal reasons for using powder metallurgy products: (1) cost savings - compared with alternative processes, and (2) unique

properties - attainable by the PM route only. By producing parts with a homogeneous structure the PM process enables manufacturers to make products that are more consistent and predictable in their behavior across a wide range of applications (Fig.1) [4].

The PM process has a high degree of flexibility allowing to forming the physical properties of a product to suit one's specific needs and performance requirements. These include, for instance: special properties like hardness and wear resistance. The unique flexibility of the PM process enables products to be made from materials that are fabricated to one's specific needs [5].

The properties of sintered parts and materials result from the interaction of three parameters: powder properties, force (pressure) and heat (time, temperature) (Fig.2). While the chemical composition and certain processing properties of powders can be varied over a wide range, the use of pressure and heat is restricted to a certain extent because of technical reasons. This also determines the limited number of applications of PM procedures in the parts production [3-5].

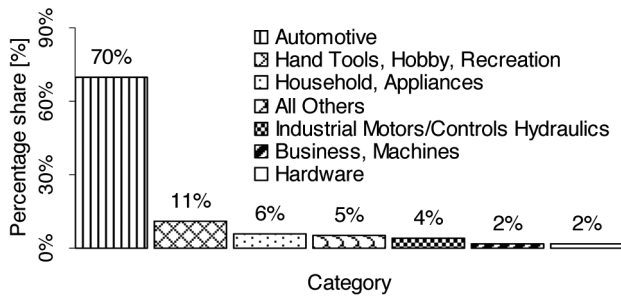


Fig. 1. Market segmentation of metal powder parts industry [4]

SINTERED COMPACT PROPERTIES	Mechanical	Chemical	Physical
	- Hardness - Yield and tensile strength - Elongation - Reduction in area bend and compression strength - Creep properties - Heat resistance - Sliding and friction properties - Wear resistance	- Composition - Purity - Gas content - Scaling resistance - Corrosion resistance - Electrochemical behaviour	- Porosity - Electrical or magnetic - Emissions - Vapour tension - Radiation absorption - Nuclear properties
SINTERED COMPACT PROPERTIES	Sintering conditions	Powder properties	Compacting conditions
	- Time - Temperature - Atmosphere (controlled vacuum) - Method (direct or indirect heating) - Heating rate	- Chemical composition - Chemical purity - Particle size - Particle size distribution - Apparent density - Particle shape - Surface properties	- Compacting pressure - Pressure application method - Compact size and shape - Lubricants

Fig. 2. Relationship between powder properties, compacting conditions, sintering conditions and sintered material properties [3]

Sinter-hardening technology was developed for P/M parts production to improve process efficiency [5]. Moreover, interest in this technology has grown, because it offers good manufacturing economy by providing a

one step process without a separate heat treatment operation and a unique combination of strength, toughness and hardness [6-9, 15-19].

Sinter-hardening typically requires that the P/M steel structure transforms itself to martensite during cooling process. Different properties and microstructure can be obtained by varying sintering cooling rates. Thanks to controlling these rates, microstructure can be designed to obtain the required amount of martensite, and desired mechanical properties [10-12, 16, 20, 24, 25, 27 - 30].

Sinter-hardening can be achieved with the use of standard sintering furnaces (for example continuous furnace) and those equipped with accelerated cooling zone (for instance vacuum furnace). The Astaloy CrL and CrM powders are examples of typical materials have been developed and used especially for sinter-hardening processes. These steel powders are mainly characteristic of higher hardenability compared with conventional P/M steels [12-14, 21 - 23, 26].

## 2. Experimental procedure

Three different systems were tested to investigate, the cooling rates effect on examined material and properties. The process of preparing materials was consisted of following stages: 1) Selection of metal powders and lubricant, 2) Mixing, 3) Compacting, 4) Debinding, 5) Sintering.

The following powders were used in the investigations:

- iron powder Astaloy CrL (Fig. 3a) and Astaloy CrM (Fig. 3b),
- lamellar graphite powder grade GR12 (Fig. 3c).

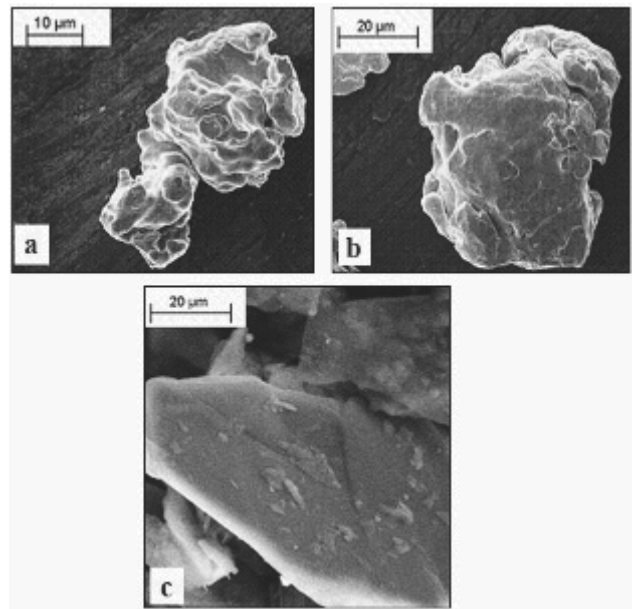


Fig. 3. Micrographs of powders: a) Astaloy CrL pre-alloyed powder, b) Astaloy CrM pre-alloyed powder, c) graphite powder (SEM)

The role of lubricant is to reduce the friction force between the powder and tool walls, and also between the particles. Just before the sintering process, the lubricant must be removed from the compact to avoid interfering with the formation and growth of bounds between the particles. Chemical composition of iron powder was presented in Table 1. The base powders are further mixed with graphite to obtain the desired strength. The amount of graphite that was admixed to the iron-base powder was 0.6% and lubricant 0.75%. The amount of graphite which is mixed with the iron-base powder is 0.6% and lubricant is 0.75%.

Table 1.

Chemical composition of iron-base powders

Base iron	Mo[%]	Cr[%]	C[%]	O <sub>2</sub> -tot[%]
Astaloy CrL	0.20	1.50	<0.01	0.16
Astaloy CrM	0.50	3.00	<0.01	0.21

## 2)Mixing

The metal powder and lubricant were mixed using two mixers. One mixture (1.6°C/s cooling rate) was mixed using a turbula mixer (20 min. 80 rpm), the other (cooling rates: 0.3 and 6.5°C/s) in a double cone laboratory mixer (20 min. 50 rpm).

## 3)Compacting

The three sets of test pieces were prepared: dog bone (Fig.4a), rectangular (10x55 for Charpy test - Fig.4b) and disk (40mm diameter for wear test - Fig.4c). The test pieces were using 200kN hydraulic press (manufactured by Uboli-Olivetti). Compacting was carried out with pressure of 500 and 600 MPa.

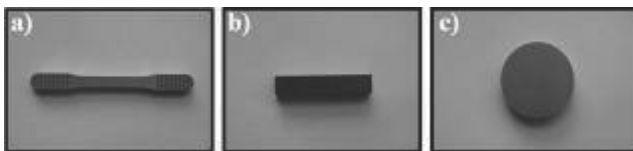


Fig. 4. Test pieces: a) dog bone, b) charpy, c) disk

## 4)Debinding

Debinding process was performed in fully nitrogen atmosphere in a separate furnace before the sintering process. Samples were kept in the furnace at 550°C for one hour to remove the possible largest fraction of lubricant.

## 5)Sintering

Sintering was performed in a vacuum furnace with argon backfilling (pressure  $5.0 \cdot 10^{-1}$  mbar). The furnace was equipped with a cooling zone to provide accelerated cooling, from the sintering temperature. Green compacts were sintered at 1120°C for 30 minutes in vacuum atmosphere and rapidly cooled in nitrogen three different rates: rapid cooling (6.5°C/s), medium cooling (1.6°C/s) and slow cooling (0.3°C/s, no gas added). All cooling rates are presented in figure 4. Green compacts were tempered in vacuum in the same furnace (at 200°C for 60 minutes) and cooled in nitrogen.

Absolute density of powders and solids in form of charpy samples (small pieces of samples) was measured on the Accu-Pyc 1330 helium apparatus in Institute for Non-ferrous Metals, Gliwice. The test based on compensation the pressure between a measurement cell with examined test pieces and a standard cell.

Microstructure was investigated using LEICA MEF4A light microscope after polishing samples and metallographic etching with Nital 2%. Moreover, powder steels and graphite morphology examination was carried out by using SEM. Observation of investigated samples was carried on using scanning electron microscopes ZEISS SUPRA 35 and OPTON DSM 940.

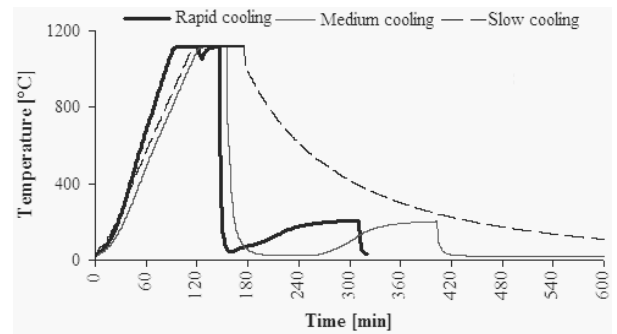


Fig. 4. Samples were sintered and cooled with three different rates

Microstructure was investigated using LEICA MEF4A light microscope after polishing samples and metallographic etching with Nital 2%. Moreover, powder steels and graphite morphology examination was carried out by using SEM. Observation of investigated samples was carried on using scanning electron microscopes ZEISS SUPRA 35 and OPTON DSM 940.

Micro hardness (HV0.1) test was done on each surface using Vickers hardness tester. Research was carried out with load of mark 100g according to standard PN-EN ISO 6507-1.

Phase composition analyses of the investigated test pieces were made on the PANalytical X'Pert PRO diffractometer, using the filtered X-ray Co K $\alpha$ , step 0.05, time counting 10 sec. at voltage of 40 kV and tube current of 30 mA.

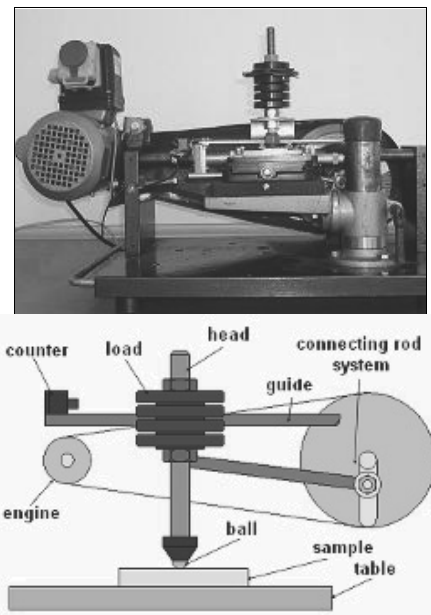


Fig. 5. The pin on plate device

The investigation of wear resistance of the tested materials was performed using the pin-on-plate machine - developed in Silesian University of Technology in Gliwice with 10 N load and different number of cycles (1000, 2000, 3000, 4000, 5000), in sequence of 22, 44, 66, 88, 110 metres. The device implements a dry friction between head with metallic ball doing reciprocating its movement of test piece. Samples were ground using the abrasive paper ( $1200 \mu\text{m}/\text{mm}^2$ ) to obtain a flat and smooth surface. Test was performed with ball made using a tungsten carbide (diameter 8.731 mm). Samples were weighed using laboratory scale before testing and after completing the cycle. Samples were washed in the ultrasonic washer to clean them and their wear was specified of based on measured mass loss and evaluated from the geometry of their wear groove.

### 3. Results and discussion

The results of the absolute density of pre-alloyed powder Astaloy CrL and Astaloy CrM measured on Accu-Pyc 1330 helium apparatus are presented in Table 2.

Table 2.  
Densities of pre-alloyed powders

Kind of powders	Number of purges	Measured value	
		Average	Stand. Deviation
Astaloy CrL	5	7.9403	0.0015
Astaloy CrM	5	7.8388	0.0013

Three different systems were tested using sinter-hardening process. The green densities for the first lot with rapid cooling were in the range from  $6.5$  to  $6.8 \text{ g}/\text{cm}^3$  (rectangular samples) and from  $6.6$  to  $6.9 \text{ g}/\text{cm}^3$  (disk samples). The sintered densities were between  $6.4$  to  $6.9 \text{ g}/\text{cm}^3$  (rectangular samples) and  $6.5$  to  $6.9 \text{ g}/\text{cm}^3$  (disk samples). The green densities for the second lot with medium cooling were included in the range from  $6.5$  to  $6.8 \text{ g}/\text{cm}^3$  (rectangular samples) and from  $6.7$  to  $6.9 \text{ g}/\text{cm}^3$  (disk samples). The sintered densities were between  $6.5$  to  $6.8 \text{ g}/\text{cm}^3$  (rectangular samples) and  $6.7$  to  $7.0 \text{ g}/\text{cm}^3$  (disk samples). The green densities for the third lot with low cooling were included in the range from  $6.5$  to  $6.9 \text{ g}/\text{cm}^3$  (rectangular samples) and from  $6.6$  to  $6.9 \text{ g}/\text{cm}^3$  (disk samples). The sintered densities were between  $6.4$  to  $6.8 \text{ g}/\text{cm}^3$  (rectangular samples) and  $6.5$  to  $6.9 \text{ g}/\text{cm}^3$  (disk samples).

Among materials with the same volume of graphite and lubricant, three highest densities, depending on cooling rate, were obtained: from both the first and third lot  $6.9 \text{ g}/\text{cm}^3$  (the steel with applied 600 MPa pressure, and Astaloy CrM powder); from the second lot –  $7.0 \text{ g}/\text{cm}^3$  (the steel with applied 600 MPa pressure, and Astaloy CrL powder). Figure 6 presents sintered densities measured with help of Accu-Pyc 1330 helium apparatus. Densities obtained after sintering are characteristic of lower values which is consistent with specification obtained from Höganäs.

The sinter-hardening process of first lot of samples, cooled with slow cooling, determined the formation of ferrite-pearlite microstructures for both Astaloy CrL and CrM ( $0.2\% \text{Mo}-1.5\% \text{Cr}-0.6\% \text{C}$ ) steels with pressures of pressing 500MPa and

600MPa. Figure 10a present microstructures after LOM analysis. Figure 11a present microstructures after LOM analysis. Figure 7 is presented XRD pattern of CrL 500MPa, rapid cooling, Fea peaks were found there.

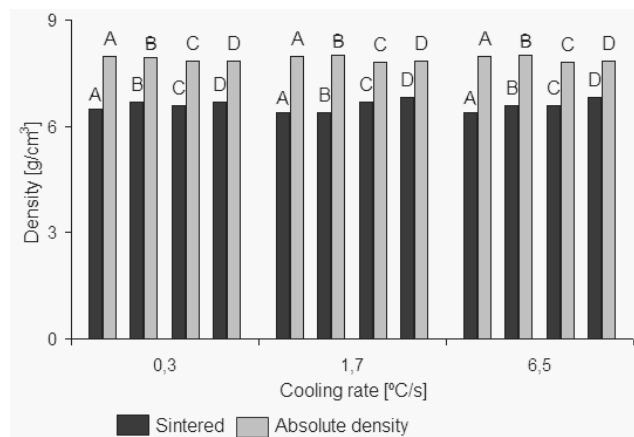


Fig. 6. Sintered and absolute density (air density according to standard atmosphere) of examined compositions (rectangular chosen samples), where: A - CrL500 MPa, B - CrL600 MPa, C - CrM500 MPa, D - CrM600 MPa

The sinter-hardening process of second lot of samples, cooled with medium cooling, determined the formation of mainly ferrite-pearlite microstructures. Microstructures obtained for Astaloy CrL( $0.2\% \text{Mo}-1.5\% \text{Cr}-0.6\% \text{C}$ ) steels with pressures of compacting 500MPa and 600MPa are presented in order a ferrite-pearlite (Fig. 10b and 11b) and ferrite-pearlite with some trucks of bainite microstructures. Microstructures obtained for Astaloy CrM( $0.5\% \text{Mo}-3\% \text{Cr}-0.6\% \text{C}$ ) steels with pressures of compacting 500MPa and 600 MPa are presented in both cases ferrite-pearlite with some amount of bainite microstructures. Figure 8 is presented XRD pattern of CrL 500 MPa, rapid cooling, Fea peaks were found.

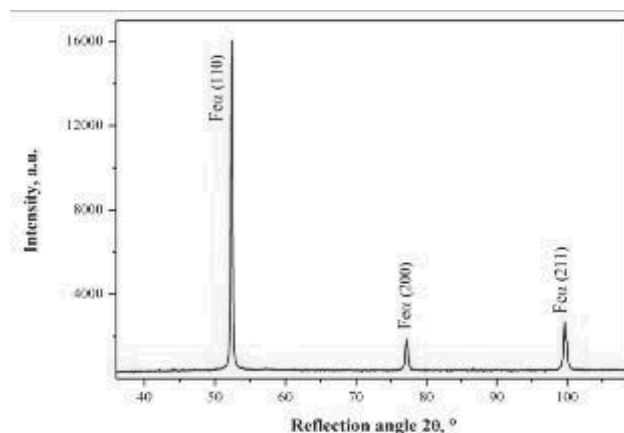


Fig. 7. X-ray diffraction pattern of CrL 500MPa, slow cooling

The sinter-hardening process of third lot of samples, cooled with rapid cooling, determined the formation of mainly martensite-bainite microstructures. Microstructures obtained for Astaloy CrL(0.2%Mo-1.5%Cr-0.6%C) steels with pressures of compacting 500MPa and 600MPa are presented in order a martensite (Fig. 10c and 11c) and martensite-bainite microstructures. Microstructures obtained for Astaloy CrM(0.5%Mo-3%Cr-0.6%C) steels with pressures of compacting 500MPa and 600MPa are presented in order bainite and martensite-bainite microstructures. Figure 9 is presented XRD pattern of CrL 500MPa, high cooling, were found  $Fe\alpha$  and  $Fe\gamma$  peaks.

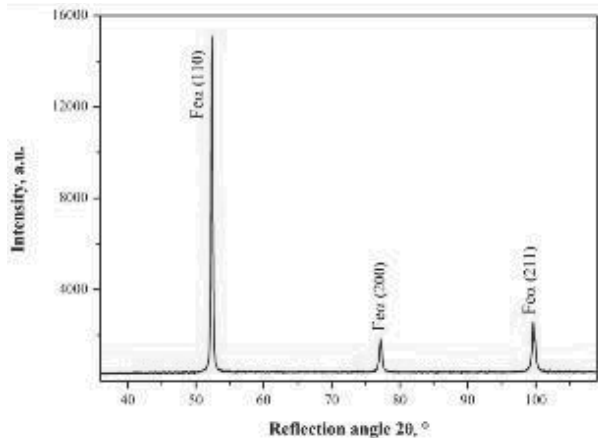


Fig. 8. X-ray diffraction pattern of CrL 500MPa, medium cooling

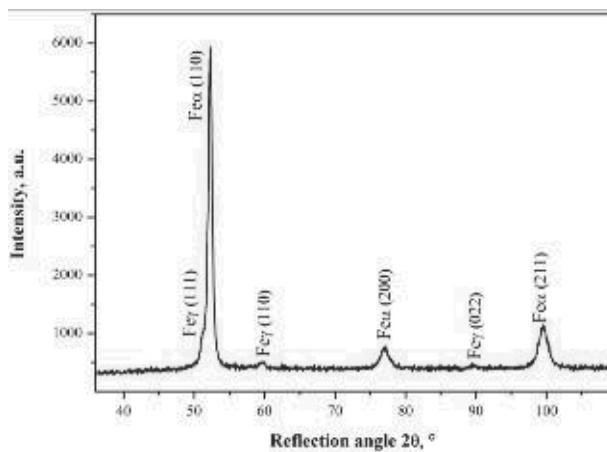
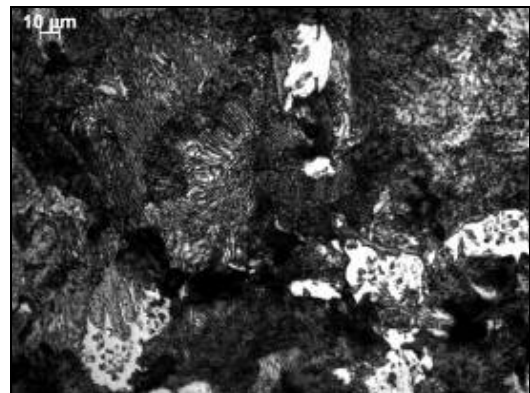


Fig. 9. X-ray diffraction pattern of CrL 500 MPa, rapid cooling

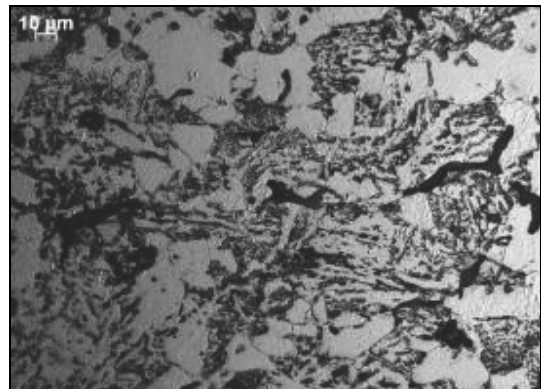
The microhardness of studied materials strongly depends on the applied kind of powder. The measurements of microhardness were performed of samples surface starting 20  $\mu\text{m}$  from the edge and continuing with the step of 100  $\mu\text{m}$  up to the center. The highest value was achieved for steel containing 0,6% C (CrL, 500 MPa, rapid cooling). The average value for this set of samples was 474.76  $\text{HV}_{0,1}$ . The max. value was 566.07  $\text{HV}_{0,1}$ . The lowest value was achieved for steel containing 0,6% C (CrL, 500 MPa, medium cooling). The average value for this set of samples was 99.91  $\text{HV}_{0,1}$ . The highest value of microhardness was achieved

for steel containing 0.6% C (CrM, 600 MPa, medium cooling), where the average was 157.91  $\text{HV}_{0,1}$  and a max. value was 181.31  $\text{HV}_{0,1}$ . The lowest value (83.72  $\text{HV}_{0,1}$ ) was achieved for steel (CrL, 500 MPa). The highest value of microhardness was achieved for steel containing 0.6% C (CrM, 600 MPa, slow cooling), where the average was 200.53  $\text{HV}_{0,1}$  and a max. value was 234.22  $\text{HV}_{0,1}$ . The lowest value (102.33  $\text{HV}_{0,1}$ ) was achieved for steel (CrL, 600 MPa).

a)



b)



c)

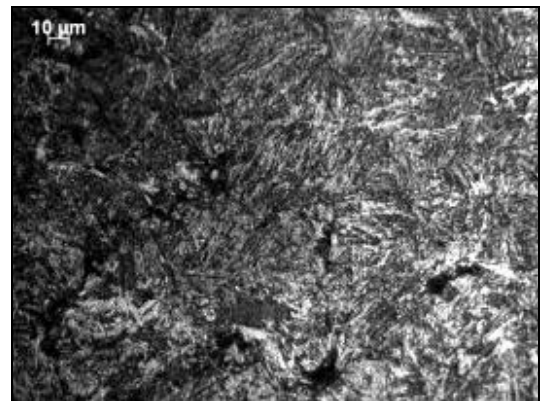


Fig. 10. Microstructure of Astaloy CrL 500MPa sintered steels: a) slow cooling; b) medium cooling; c) rapid cooling; light optical microscopy (LOM)

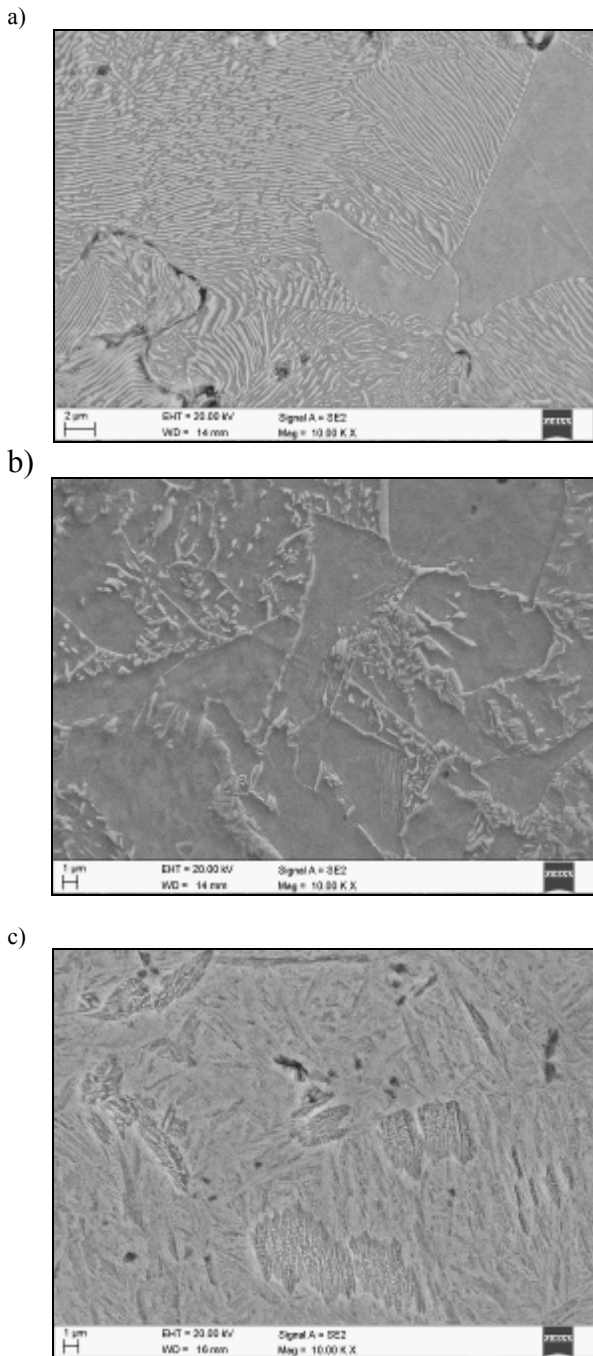


Fig. 11. Microstructure of Astaloy CrL 500MPa sintered steels: d) slow cooling; e) medium cooling; f) rapid cooling; SEM

The microhardness of studied materials strongly depends on the applied kind of powder. The measurements of microhardness were performed of samples surface starting 20  $\mu\text{m}$  from the edge and continuing with the step of 100  $\mu\text{m}$  up to the center. The highest value was achieved for steel containing 0,6% C (CrL, 500

MPa, rapid cooling). The average value for this set of samples was 474.76  $\text{HV}_{0,1}$ . The max. value was 566.07  $\text{HV}_{0,1}$ . The lowest value was achieved for steel containing 0.6% C (CrL, 500 MPa, medium cooling). The average value for this set of samples was 99.91  $\text{HV}_{0,1}$ . The highest value of microhardness was achieved for steel containing 0.6% C (CrM, 600 MPa, medium cooling), where the average was 157.91  $\text{HV}_{0,1}$  and a max. value was 181.31  $\text{HV}_{0,1}$ . The lowest value (83.72  $\text{HV}_{0,1}$ ) was achieved for steel (CrL, 500 MPa). The highest value of microhardness was achieved for steel containing 0.6% C (CrM, 600 MPa, slow cooling), where the average was 200.53  $\text{HV}_{0,1}$  and a max. value was 234.22  $\text{HV}_{0,1}$ . The lowest value (102.33  $\text{HV}_{0,1}$ ) was achieved for steel (CrL, 600 MPa).

There are slight differences between results of measurement for steels cooled on two cooling rates slow and medium. We can classify these results into two cases. However, there are significant differences between results of measurement for steels cooled with these cases and rapid cooling. These all differences could have come from porosity, which characterised these materials. Comparable results obtained in the case of slow and medium cooling rate (mainly ferrite-pearlite structures or inversely proportional). Figure 12 presents microhardness of studied materials.

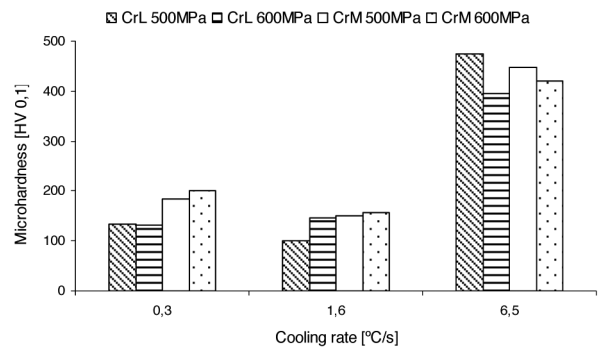


Fig. 12. Microhardness in versus cooling rate; average values

The next step was to measure the wear resistance. Figures from 13 to 15 present relationship percentage loss of mass depending on sliding distance and kind of cooled material with different rates.

In the first case (steel cooled with slow cooling) it was found that the maximum wear is characteristic of Astaloy CrL 500 MPa steel sample, after traversed 110 m (it is 0,045%) (Fig. 13). Whereas the minimum wear (it is 0.0085%) is characteristic of a steel sample from Astaloy CrM 600 MPa. There was found that the minimum wear of abrasive ball took place during cooperation with steel samples of Astaloy CrL i CrM pressing under 600MPa pressure.

In the second case (steel cooled with medium cooling) it was found that the maximum wear (it is 0.038%) is characteristic of Astaloy CrM 500MPa steel sample (Fig. 14). Whereas the minimum wear (it is 0.0078%) is characteristic of a steel sample from Astaloy CrM 600MPa. There was observed that during tests an abrasive ball was wear insignificant in case of cooperating with the minimum wear of abrasive ball took place during cooperation with Astaloy CrL 500 and 600MPa steel samples, but it does not give in to

wear during cooperation with Astaloy CrM 500 and 600MPa steel samples.

In the third case (steel cooled with rapid cooling) it was found that the maximum wear (it is 0.0082%) is characteristic of Astaloy CrM 600MPa steel sample (Fig. 15). While the minimum wear (it is 0.0052%) is characteristic of a steel sample from Astaloy CrL 500MPa. In case materials cooled with this rate, it was found a mass allowance of abrasive ball, after cooperating with Astaloy CrL 500 and 600MPa materials, what was caused by adhering threadbare file dusts of sample on a surface of abrasive ball during weighing.

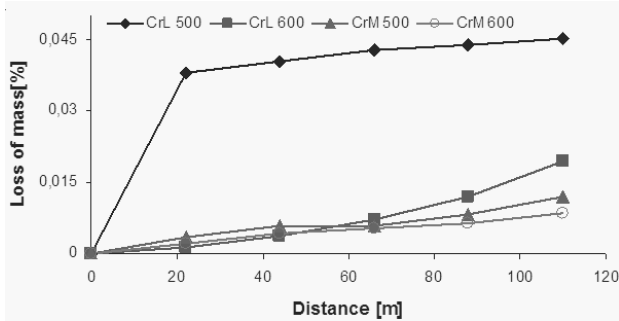


Fig. 13. Loss of mass in versus sliding distance for the steel cooled with slow cooling

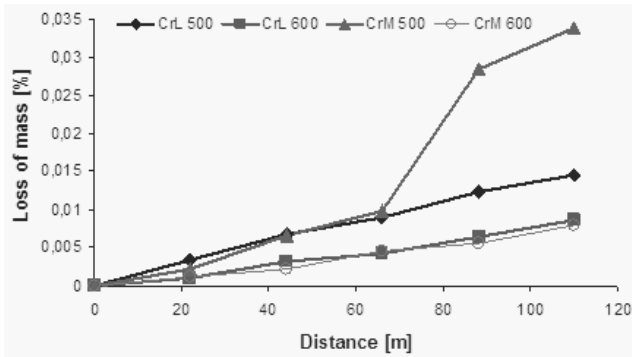


Fig. 14. Loss of mass in versus sliding distance for the steel cooled with medium cooling

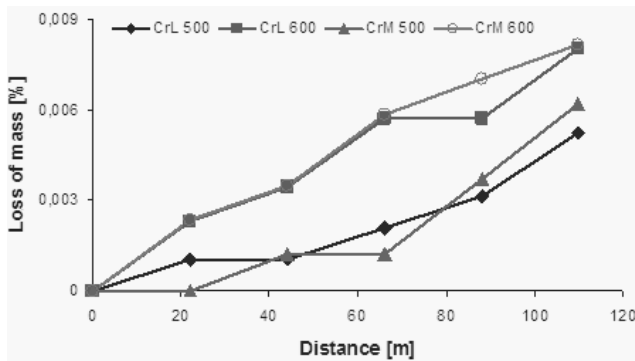


Fig. 15. Loss of mass in versus sliding distance for the steel cooled with high cooling

Next, calculations were carried out on the based wiped groove of dimension (Fig.16), obtaining in this way geometrical loss of mass. Data shown were illustrated on Figures from 17 to 19. Comparing obtained results of geometrical loss of mass with actual one, it was found that the accuracy results of geometrical method is contingent on accuracy performing length and width measurements of wiped groove, moreover analytical results are higher than real calculations. However, making general comparison both methods first and second, it was found that they indicated similarly, which of materials is more resistant to abrasion.

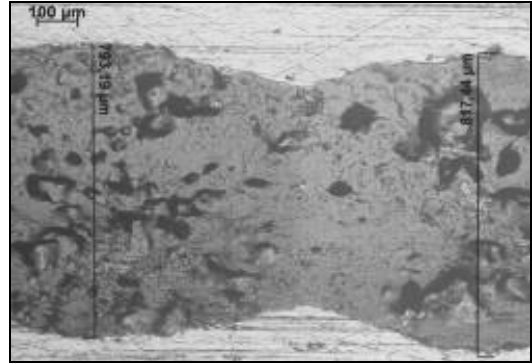


Fig. 16. Micrograph of wiped groove dimensions

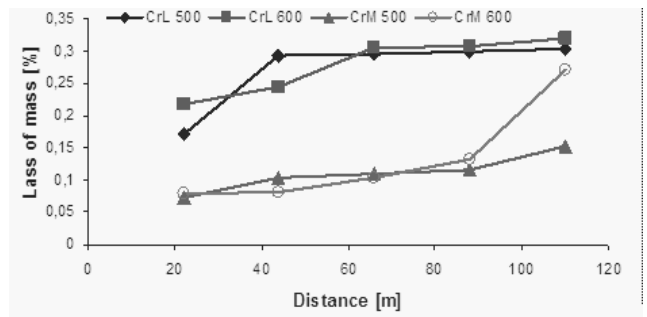


Fig. 17. Geometrical loss in versus sliding distance for the steel cooled with slow cooling

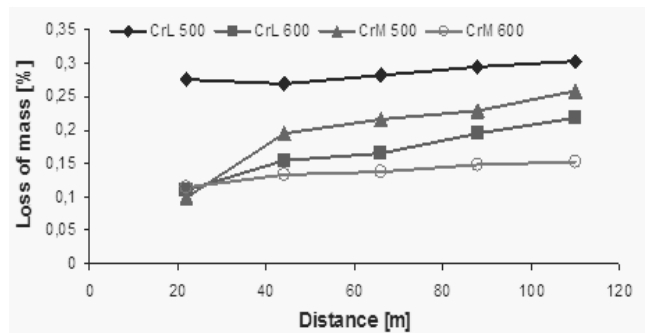


Fig. 18. Geometrical loss of mass in a function of sliding distance for the steel cooled with medium cooling

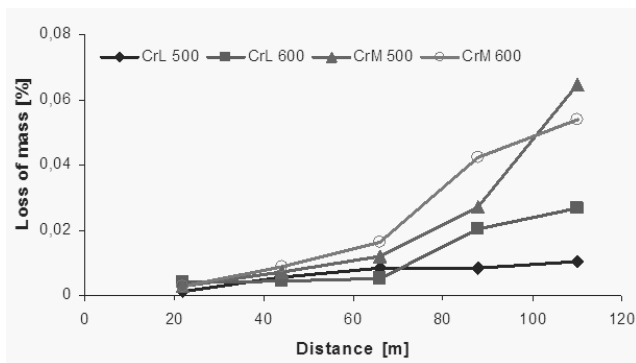


Fig. 19. Geometrical loss of mass in a function of sliding distance for the steel cooled with rapid cooling

## 4. Summary

Investigations of CrL and CrM sintered steels alloys proved that: application of different cooling rates effecting on the formation of different microstructures and because of this, also on properties. It was observed that a rapid cooling rate provides higher materials wear resistance than the medium and slow cooling rate. The highest value was obtained for a CrM 600MPa sample (rapid cooling) for wear resistance test (using pin on plate). The highest value was obtained for a CrM 500MPa sample (rapid cooling) for wear resistance, where calculations were carried out. The actual method of mass loss in comparison with a geometrical method gives precise results, because it is not burdened with any simplifications and its precision depends from accuracy of laboratory balance only. Higher cooling rate is directly influencing the structure of tested samples. Those which were cooled down with a higher cooling rate have a martensitic structure and those with medium cooling rate have a ferrite-pearlite microstructure (CrM 600MPa sample), with slow cooling rate has a ferrite-pearlite microstructure with some amount of bainite microstructures (CrM 600MPa sample).

## Acknowledgements

Investigations were partially realized within the framework of the Erasmus Programme, in Politecnico di Torino, Campus Alessandria, Italy. Authors of this paper would like to thank M. Rosso, M. Actis Grande for making materials available for annual investigations and for cooperation.

## References

- [1] The ASM Powder Metallurgy Committee, Metals Handbook, 9 edition, 7, 1984, 9.
- [2] <http://epma.autotrain.org>
- [3] A. Šalák, Ferrous powder metallurgy, Cambridge International Science Publishing, England 1995, 45-46.
- [4] K.S. Narasimhan, Sintering of powder mixtures and the growth of ferrous powder metallurgy, Materials Chemistry and Physics, 67 (2001) 56-65.
- [5] M.C. Baran, A.H. Graham, A.B. Davala, R.J. Causton, C. Schade Hoeganaes Corporation, A superior sinter-hardenable material, International Conference on Powder Metallurgy and Particulate Materials 20-24 (1999) 1-19.
- [6] G.H. Rutz, A.H. Graham, A.B. Davala, Sinter-hardening P/M. steels, Proceedings of the International Conference on Powder Metallurgy and Particulate Materials, Chicago 1997.
- [7] L.A. Dobrzański, J. Otręba, M. Actis Grande, M.Rosso, Sinter-hardening of Ni-Mo pre-alloyed powders with tungsten addition, Jurnal of Achievements in Materials and Manufacturing Engineering, 20/1-2 (2007) 427-430.
- [8] M. L. Marucci, G. Fillari, P. King, K. S. Sim Narashiman, Sintering a path to cost-effective hardened parts, Metal Powder Report 60 (2005) 42-46.
- [9] L.A. Dobrzański J. Otręba, M. Actis Grande, M.Rosso, Sinter-hardening of Ni-Mo-W steels and their properties, Archives of Materials Science and Engineering 28/2 (2007) 77-82.
- [10] L.A. Dobrzański, J. Otręba, M. Actis Grande, M.Rosso, Microstructural characteristic and mechanical properties of Ni-Mo-(W) steels, Journal of Achievements in Materials and Manufacturing Engineering 18/1-2 (2006) 347-350.
- [11] E. Akpan, Sinter-hardening PM materials and nature of process, Industrial Heating 61/5 (1994) 41-43.
- [12] B. Llindsley, T. Murphy, Dimensional precision in sinter-hardening PM steels, Materials Science Forum, 534-536/1, (2007), 665-8.
- [13] S. St-Laurent, P. Lemieux, S. Pelletier, Behavior of sinter hardening powders during sintering, Proceedings of the International Conference on Powder Metallurgy and Particulate Materials 10, 2004, 145-159.
- [14] G.H. Rutz, H.A. Graham, B.A. Davala, Sinter-hardening P/M. steels, Advances in Powder Metallurgy and Particulate Materials 1 (1997) 8-3-8-20.
- [15] L.A. Dobrzański, J. Hajduczek, A. Kloc-Ptaszna, Effect of the sintering parameters on structure of the gradient tool materials. Journal of Achievements in Materials and Manufacturing Engineering 36/1 (2009) 33-40.
- [16] Z. Brytan, L.A. Dobrzański, M. Actis Grande, M. Rosso, Characteristics of vacuum sintered stainless steels, Journal of Achievements in Materials and Manufacturing Engineering 33/2 (2009) 126-134.
- [17] G. Matula, K. Golombek, J. Mikula, L.A. Dobrzański, Structure of sintered gradient tool materials, Journal of Achievements in Materials and Manufacturing Engineering 32/1 (2009) 23-28.
- [18] R. Yilmaz, M.R. Ekici, Microstructural and hardness characterisation of sintered low alloyed steel, Journal of Achievements in Materials and Manufacturing Engineering 31/1 (2008) 23-28.
- [19] G. Matula, L.A. Dobrzański, A. Varez, B. Levenfeld, Development of a feedstock formulation based on PP for MIM of carbides reinforced M2, Journal of Achievements in Materials and Manufacturing Engineering 27/2 (2008) 195-198.
- [20] L.A. Dobrzański, Z. Brytan, M. Rosso, Sinter-hardening process applicable to stainless steels, Journal of Achievements in Materials and Manufacturing Engineering 24/2 (2007) 11-18.

- [21] L.A. Dobrzański, A. Kloc-Ptaszna, G. Matula, J.M. Contreras, J.M. Torralba, The impact of production methods on the properties of gradient tool materials, *Journal of Achievements in Materials and Manufacturing Engineering* 24/2 (2007) 19-26.
- [22] L.A. Dobrzański, A. Kloc-Ptaszna, G. Matula, J.M. Torralba, Structure and properties of gradient tool materials with the highspeed steel matrix, *Journal of Achievements in Materials and Manufacturing Engineering* 24/2 (2007) 47-50.
- [23] G. Matula, L.A. Dobrzański, G. Herranz, A. Varez, B. Levenfeld, J.M. Torralba, Structure and properties of HS6-5-2 type HSS manufactured by different P/M methods, *Journal of Achievements in Materials and Manufacturing Engineering* 24/2 (2007) 71-74.
- [24] L.A. Dobrzański, J. Otreba, Z. Brytan, M. Rosso, Utilisation of sinter-hardening treatment for various sintered steels, *Journal of Achievements in Materials and Manufacturing Engineering* 24/2 (2007) 187-190.
- [25] M. Rosso, Contribution to study and development of PM stainless steels with improved properties, *Journal of Achievements in Materials and Manufacturing Engineering* 24/1 (2007) 178-187.
- [26] L.A. Dobrzański, A. Kloc-Ptaszna, A. Dybowska, G. Matula, E. Gordo, J.M. Torralba, Effect of WC concentration on structure and properties of the gradient tool materials, *Journal of Achievements in Materials and Manufacturing Engineering* 20 (2007) 91-94.
- [27] L.A. Dobrzański, Z. Brytan, M. Actis Grande, M. Rosso, Influence of sintering parameters on the properties of duplex stainless steel, *Journal of Achievements in Materials and Manufacturing Engineering* 20 (2007) 231-234.
- [28] L.A. Dobrzański, Z. Brytan, M. Actis Grande, M. Rosso, Corrosion resistance properties of sintered duplex stainless steel, *Journal of Achievements in Materials and Manufacturing Engineering* 19/1 (2006) 38-45.
- [29] L.A. Dobrzański, M. Musztyfaga, M. Actis Grande, M. Rosso, Computer aided determination of porosity in sintered steels, *Archives of Materials Science and Engineering* 38/2 (2009) 103-111.
- [30] M. Rosso, L.A. Dobrzański, J. Otreba, M. Actis Grande, Mechanical properties and microstructural characteristic of sinter-hardened steels, *Archives of Materials Science and Engineering* 35/2 (2009) 117-124.